A novel cross-species model of Barlow's disease to biomechanically analyze repair techniques in an ex vivo left heart simulator

Annabel M. Imbrie-Moore, MS,[a,b] Michael J. Paulsen, MD,[a] Yuanjia Zhu, MD,[a,c] Hanjay Wang, MD,[a] Haley J. Lucian, BA,[a] Justin M. Farry, BSE,[a] John W. MacArthur, MD,[a] Michael Ma, MD,[a] and Y. Joseph Woo, MD[a,c]

ABSTRACT

Objective: Barlow's disease remains challenging to repair, given the complex valvular morphology and lack of quantitative data to compare techniques. Although there have been recent strides in ex vivo evaluation of cardiac mechanics, to our knowledge, there is no disease model that accurately simulates the morphology and pathophysiology of Barlow's disease. The purpose of this study was to design such a model.

Methods: To simulate Barlow's disease, a cross-species ex vivo model was developed. Bovine mitral valves (n = 4) were sewn into a porcine annulus mount to create excess leaflet tissue and elongated chordae. A heart simulator generated physiologic conditions while hemodynamic data, high-speed videography, and chordal force measurements were collected. The regurgitant valves were repaired using nonresectional repair techniques such as neochord placement.

Results: The model successfully imitated the complexities of Barlow's disease, including redundant, billowing bileaflet tissues with notable regurgitation. After repair, hemodynamic data confirmed reduction of mitral leakage volume (25.9 ± 2.9 vs 2.1 ± 1.8 mL, $P < .001$) and strain gauge analysis revealed lower primary chordae forces (0.51 ± 0.17 vs 0.10 ± 0.05 N, $P < .001$). In addition, the maximum rate of change of force was significantly lower postrepair for both primary (30.80 ± 11.38 vs 8.59 ± 4.83 N/s, $P < .001$) and secondary chordae (33.52 ± 10.59 vs 19.07 ± 7.00 N/s, $P = .006$).

Conclusions: This study provides insight into the biomechanics of Barlow's disease, including sharply fluctuating force profiles experienced by elongated chordae prerepair, as well as restoration of primary chordae forces postrepair. Our disease model facilitates further in-depth analyses to optimize the repair of Barlow's disease. (J Thorac Cardiovasc Surg 2021;161:1776-83)

Novel cross-species model simulates Barlow's disease for ex vivo biomechanical analysis.

CENTRAL MESSAGE

A cross-species ex vivo model simulates Barlow's disease and provides insight into the biomechanics of the disease and surgical repair.

PERSPECTIVE

Ex vivo heart simulation can provide vital quantitative biomechanical analyses of valve repair techniques. However, there is a need for disease models that reproduce the complex morphology of severe mitral valve disease to support this surgical optimization. Our cross-species model successfully simulates Barlow's disease and will enable a comprehensive analysis of the numerous repair techniques.

See Commentaries on pages 1784 and 1786.

Degenerative mitral valve (MV) disease exists on a spectrum of severity, ranging from relatively mild disease with chordal rupture or elongation, termed fibroelastic deficiency, to profound myxomatous degeneration of the valve, with elongated chordae and excessive, thickened, and redundant leaflet tissue, termed Barlow's disease. First described by John B. Barlow,[1] Barlow's disease is a severe degenerative MV disease characterized by excess and billowing leaflet tissue, single-leaflet or bileaflet prolapse, annular dilatation, and elongated chordae.[2-4] This

From the Departments of [a]Cardiothoracic Surgery, [b]Mechanical Engineering, and [c]Bioengineering, Stanford University, Stanford, Calif.

A. M. Imbrie-Moore and M. J. Paulsencontributed equally to this article.

This work was supported in part by the National Institutes of Health (NIH R01 HL089315-01, Y.J.W.), the American Heart Association (17POST33410497, M.J.P.), the National Science Foundation Graduate Research Fellowship Program (A.M.I.), a Stanford Graduate Fellowship (A.M.I.), and generous support from Donald and Sally O'Neal. The content is solely the responsibility of the authors and does not necessarily represent the official views of the funders.

Received for publication Oct 10, 2019; revisions received Dec 17, 2019; accepted for publication Jan 2, 2020; available ahead of print Feb 19, 2020.

Address for reprints: Y. Joseph Woo, MD, Departments of Cardiothoracic Surgery and Bioengineering, Stanford University, Falk Cardiovascular Research Building CV-235, 300 Pasteur Dr, Stanford, CA 94305-5407 (E-mail: joswoo@stanford.edu).

0022-5223/$36.00

https://doi.org/10.1016/j.jtcvs.2020.01.086

Abbreviations and Acronyms
3D = 3-dimensional
dF/dt = rate of change of force with respect to time
FBG = fiber Bragg grating
MV = mitral valve

Scanning this QR code will take you to the table of contents to access supplementary information.

complex morphology with significant disparity from a healthy MV can be challenging to repair surgically, and the optimal technique for repairing Barlow's disease remains in question.

Current surgical techniques that may be applied in the repair of Barlow's disease include annuloplasty, leaflet resection, neochord placement, chordal transfer, and nonresectional leaflet remodeling, among others.[5-10] Ex vivo heart simulators have previously been successfully used to analyze, optimize, and design new surgical techniques for MV repair.[11-17] The majority of these studies use porcine MVs as a human analog.[16,18-22] This is due to the similarities between human and porcine valves, including comparable size, anatomy, tissue microstructures, and anisotropy.[16,23,24] Simple modifications to healthy porcine or ovine MVs can be used to create mitral regurgitation models via chordae tendineae transection, annular dilatation, or papillary muscle manipulation. However, an explanted healthy porcine or ovine MV is insufficient to model the thickened, redundant leaflets and elongated chordae tendineae characteristic of Barlow's disease. For this reason, ex vivo studies aimed at comparing surgical techniques to determine the optimal repair strategy for Barlow's disease have not been performed. The development of a novel disease model that can capture the multifaceted characteristics of Barlow's disease would enable a full biomechanical analysis of the Barlow's MV and ultimately provide quantitative insight regarding the surgical repair. In this manuscript, we aimed to develop such a model.

METHODS

Model Design

To confirm that there was no previous disease model that accurately simulates the morphology and pathophysiology of Barlow's disease, a comprehensive search of PubMed was performed for the following key words: ("Ex vivo" OR "In vitro") AND ("Barlow" OR "mitral regurgitation") AND ("disease model" OR "model"). This yielded 97 results, which we carefully reviewed and found no disease model for in vitro or ex vivo use replicating Barlow's disease. To develop an accurate simulation of Barlow's disease, the model MV must have excess, thickened leaflet tissue relative to annulus size, as well as elongated chordae. Bovine MVs were selected as the basis for the model, as they provide the necessary excess leaflet tissue and chordal length relative to a human or porcine annulus. Fresh bovine hearts were obtained from a local abattoir, and the MVs were carefully excised to preserve the annulus, leaflets, papillary muscles, and chordae.

The valves were sewn to a custom 3-dimensional (3D)-printed silicone mounting rings (Carbon M2; Carbon 3D Inc, Redwood City, Calif), which were positioned between the left atrial and left ventricular chambers of a left heart simulator—described in the next section. Note that the mounting ring material allows for elasticity of the attachment point to reduce fixation of the annulus. The ring was sized as it would be for a normal porcine valve with an intercommisural distance of 30 mm. However, the posterior portion of the ring, where the posterior annulus was affixed, was made to incorporate additional circumferential distance with a geometry simulating that of a Barlow's MV annulus.[2] Due to the reduced size of the mounting ring compared with the bovine annulus, additional care was taken in securing the valve at the level of the mitral annulus onto the mounting ring using at least 8 interrupted 2-0 braided polyester sutures for uniform reduction of annular size. A continuous running 2-0 polypropylene suture was then used along the underside of the valve around the left atrial tissue to create a hemostatic suture line.

Papillary muscles were positioned to model elongated chordae typically found in Barlow's disease. For each valve, the papillary muscles were fixed to silicone holders and instrumented within the simulator as previously described,[17] but their positions were raised relative to their native state. The adjustable displacement of the bovine papillary muscles enables our disease model to be actively modulated by researchers to create the desired degree of mitral regurgitation for a given Barlow's disease model. To produce a lower regurgitation fraction, the papillary muscles can be displaced by a small margin and the annulus mount can be sized closer to the native bovine annulus size; for greater regurgitation, the papillary muscles can be raised more significantly and the annulus mount size discrepancy can be sized larger.

For consistency in this study, optimal papillary muscle placement was determined through a combination of methods. First, the gross position of the papillary muscles was estimated based on measurements taken from the valve prior to it being explanted from the porcine heart. Next, we shortened this to a range typically found in human patients.[25] We verified appropriate bileaflet prolapse typical of the clinical disease both visually and with echocardiography. To assure the creation of moderate-to-severe mitral regurgitation, we ensured that the electromagnetic flow meter readings showed a regurgitant fraction of 35% to 50%. The regurgitant valve was then repaired by experienced cardiac surgeons using nonresectional mitral repair techniques, primarily via neochord placement using multiple double-armed polytetrafluoroethylene suture (Gore-Tex Suture; WL Gore & Associates Inc, Flagstaff, Ariz). To minimize confounding factors, ring annuloplasty was not performed in these experiments, which simulates preannuloplasty ring repair testing.

Left Heart Simulator

We designed and built a 3D-printed left heart simulator, which has been described previously.[16,17,26,27] The simulator features a custom left ventricular chamber mounted to a programmable pulsatile linear piston pump (ViVitro Superpump; ViVitro Labs, Victoria, BC, Canada). The simulator includes ventricular, aortic, and left atrial pressure transducers (Utah Medical Products Inc, Midvale, Utah) as well as electromagnetic flow probes (Carolina Medical Electronics, East Bend, NC). To ensure proper transduction of the flow meters, 0.9% normal saline was used as the test fluid and held at 37°C. A 29-mm mechanical aortic valve (St Jude Regent; Abbott Vascular, Lake Bluff, Ill) was placed in the aortic position. The pump was programmed to produce a physiologic waveform

ADULT

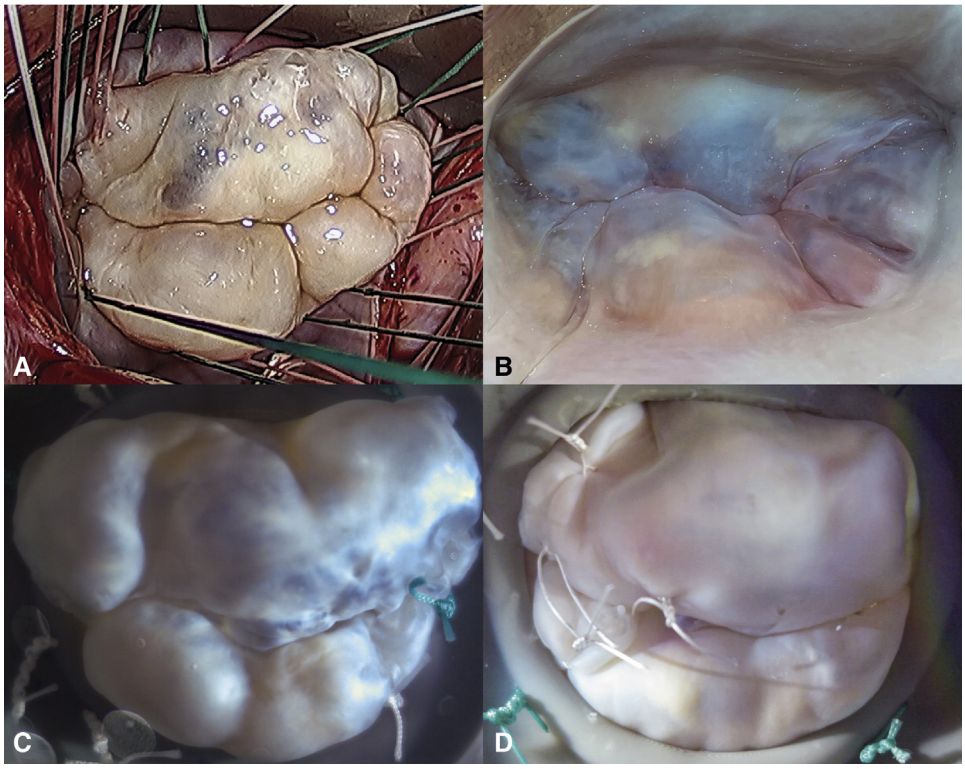

FIGURE 1. A, Intraoperative example of human Barlow's disease. B, A bovine valve in its native pressurized state, for reference to compare with the ex vivo Barlow's disease model. C, Explanted bovine valve sewn into a porcine-sized mounting ring to simulate Barlow's disease; valve pictured during systole in a left heart simulator with a leakage volume of 28.3 mL. D, A Barlow's disease model valve after neochordal repair prior to annuloplasty with a leakage volume of 3.4 mL.

in compliance with ISO 5840 standards for in vitro valve testing. Peripheral resistance and compliance in the system were initially titrated with a 28-mm leakless disc valve (ViVitro) in the mitral position to generate a cardiac output of 5 L/min, a systolic pressure of 120 mm Hg, and a diastolic pressure of 80 mm Hg. During testing, the mechanical MV was replaced by the Barlow's disease model valve, and in each phase 10 cycles of hemodynamic data were collected and averaged. Leakage volume was calculated as the volume of flow leaking across the valve post–valve closure during systole. Echocardiographic data were obtained with a Philips iE33 system (Philips, Bothell, Wash) with an X7-2T transesophageal probe from a ventricular chamber port so that the ultrasound beam was parallel to the direction of flow.

Chordae Force Measurement

Forces on the chordae tendineae were measured with fiber Bragg grating (FBG) strain gauge sensors (DTG-LBL-1550 125 μm; FBGS International, Geel, Belgium), calibrated to correlate measured strains to forces, as previously described.[17,26,27] In brief, FBGs are low-mass optical strain gauges with a thin profile, enabling the instrumentation of multiple chordae without disrupting the hemodynamics and structural integrity of the valve. The sensors were fixed to native primary and secondary chordae using CV-5 to CV-7 polytetrafluoroethylene (depending on chordal diameter) flanking each side of the 5-mm strain gauge. Once attached, the section of chordae between the sutures was severed so all force on the chordae was imparted to the FBG sensor. Multiple native chordae (n = 5-6) were instrumented for each valve, including primary and secondary chordae in both posterior and anterior positions. Maximum chordal forces over a cardiac cycle were calculated as well as the rate of change of force with respect to time (dF/dt).

Statistical Analysis

Statistical significance was defined at $P < .05$ for all tests. Hemodynamic and chordal force variables are reported as mean ± standard

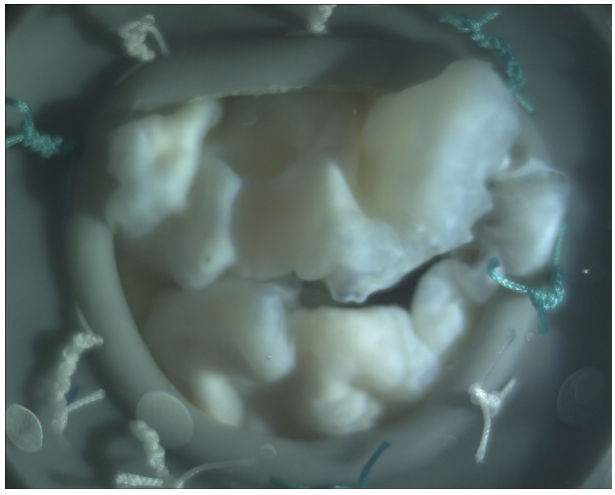

VIDEO 1. High-speed video (1057 frames per second) of a bovine mitral valve sewn to a porcine mount in a left heart simulator as a novel disease model for human Barlow's disease. Video available at: https://www.jtcvs.org/article/S0022-5223(20)30437-2/fulltext.

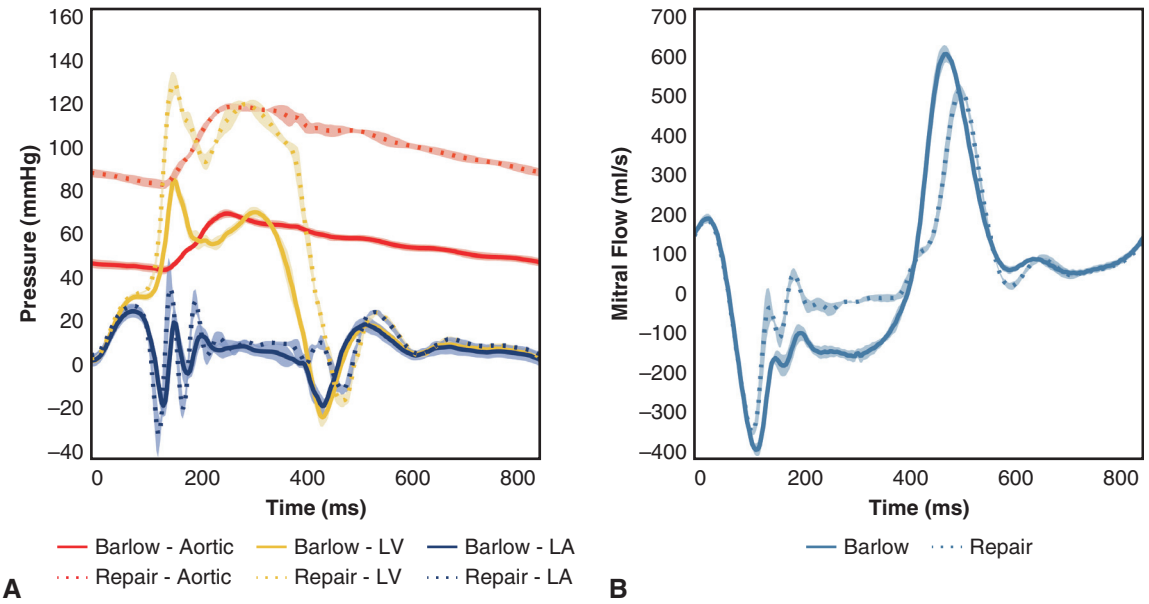

FIGURE 2. A, Mean flow confirmed successful repair of the Barlow's disease model with significantly lower leakage volumes after neochordal repair (25.9 ± 2.9 mL vs 2.1 ± 1.8 mL, $P < .001$). The *shaded region* represents standard deviation. B, Mean pressure tracings also showed successful repair of the Barlow's disease model with aortic and left ventricular pressures significantly raised to baseline levels—see Table 1 for hemodynamic values. *LV*, Left ventricular; *LA*, left atrial.

deviation. The Shapiro–Wilk statistic was used to assess normality, with each group of data assumed to be normally distributed for $P < .05$. In all cases, normality was satisfied and thus prerepair and postrepair continuous variables were compared using a paired-samples t test. Maximum chordal forces were calculated as the average force during systole and normalized to transmitral mean pressure.

RESULTS

Bovine hearts (n = 4) were tested in the porcine mounts, and the resulting disease model closely simulated the human Barlow's MV with the characteristic prolapsed and billowing bileaflet tissue and elongated chordae that caused significant mitral regurgitation. En face views of the cross-species model are shown in Figure 1 with an intraoperative view of a human Barlow's MV (Figure 1, *A*) for reference. As a comparison, Figure 1, *B,* represents an example of a bovine MV in a pressurized native state before explantation. Figure 1, *C,* shows a representative Barlow's disease model valve with a leakage volume of 28.3 mL after implanting the bovine valve in a porcine-sized annulus, showing the significant morphologic change induced by our cross-species model design. This model is also shown in a high-speed video at 1057 frames per second (Video 1). The redundant leaflet tissue and significant prolapse seen in Figure 1, *C,* were observed in all of the disease model valves. Neochordal repair was successfully performed by experienced cardiac surgeons on all valves. Figure 1, *D,* shows a Barlow's disease model valve after neochordal repair with a leakage volume of 3.4 mL. Echocardiography confirmed that in all cases prerepair, the prolapse was multisegmental and involved both leaflets; postrepair, the degree of prolapse and billowing was reduced and the coaptation area increased.

Mean mitral flow tracings and pressure tracings of the Barlow's model pre- and postrepair are shown in Figure 2. Hemodynamic and chordae tension parameters are displayed in Table 1. Flow data confirmed that neochordal repair significantly reduced mitral leakage volume in the valves from 25.9 ± 2.9 mL to 2.1 ± 1.8 mL ($P < .001$). Pressure data also confirmed successful repair with significantly greater systolic pressure ($P < .001$), diastolic pressure ($P < .001$), and left ventricular pressure ($P < .001$) postrepair.

By restoring coaptation and reducing the leakage volume, neochordal repair resulted in significantly lowered forces on primary chordae (0.51 ± 0.17 N vs 0.10 ± 0.05 N, $P < .001$). No significant difference was found for secondary chordae forces pre- versus postrepair (0.41 ± 0.21 vs 0.35 ± 0.12 N, $P = .374$). The maximum rate of change of force was also found to be significantly decreased after repair of the valve for both primary chordae (30.80 ± 11.38 N/s vs 8.59 ± 4.83 N/s, $P < .001$) and secondary chordae (33.52 ± 10.59 N/s vs 19.07 ± 7.00 N/s, $P = .006$). Composite force tracings for each class of chordae tendineae also revealed a qualitative difference in the force profiles of the Barlow's model between the prerepair (Figure 3, *A*) and the postrepair state (Figure 3, *B*): there appears to be greater fluctuation in the chordal forces during systole in the Barlow's model, and the fluctuation is consistent across valves such that it remains prominent in the composite tracings.

TABLE 1. Hemodynamic and chordae tendineae tension parameters

	Barlow's model	Repair	*P* value
Hemodynamics			
Heart rate, bpm	70.00 ± 0.00	70.00 ± 0.00	1.0000
Mean arterial pressure, mm Hg	54.97 ± 1.49	99.85 ± 1.22	**<.001**
Diastolic pressure, mm Hg	43.29 ± 2.17	81.67 ± 1.64	**<.001**
Systolic pressure, mm Hg	69.98 ± 1.91	119.53 ± 1.54	**<.001**
Mean atrial pressure, mm Hg	7.90 ± 2.80	10.55 ± 0.70	.0901
Mean ventricular pressure, mm Hg	25.82 ± 1.31	44.14 ± 0.92	**<.001**
Cardiac output, L/min	3.04 ± 0.28	4.23 ± 0.15	**.0077**
Effective stroke volume, mL	43.44 ± 3.99	60.50 ± 2.19	**.0077**
Pump stroke volume, mL	109.82 ± 0.04	109.81 ± 0.19	.9658
Mitral valve mean gradient, mm Hg	–0.47 ± 1.65	–3.80 ± 1.59	**.0187**
Mitral valve mean back pressure, mm Hg	51.71 ± 3.97	98.50 ± 2.23	**<.001**
Mitral forward flow time, s	0.52 ± 0.01	0.53 ± 0.01	.2620
Mitral forward volume, mL	92.03 ± 5.58	76.56 ± 1.58	**.0102**
Mitral valve RMS forward flow, mL/s	246.86 ± 12.41	202.78 ± 5.06	**.0026**
Mitral regurgitant fraction, %	52.85 ± 1.80	20.98 ± 2.30	**<.001**
Mitral leakage rate, mL/s	–112.88 ± 12.99	–8.15 ± 8.45	**<.001**
Mitral leakage volume, mL	–25.88 ± 2.92	–2.14 ± 1.79	**<.001**
Mitral closing volume, mL	–22.70 ± 1.16	–14.07 ± 1.73	**<.001**
Ventricular energy, mJ	673.54 ± 16.64	885.22 ± 43.25	**<.001**
Transmitral forward energy loss, mJ	16.10 ± 19.23	2.18 ± 13.87	**.0011**
Transmitral closing energy loss, mJ	105.54 ± 8.05	58.85 ± 12.92	**.0197**
Transmitral leakage energy loss, mJ	187.67 ± 32.00	31.28 ± 29.37	**<.001**
Transmitral total energy loss, mJ	309.30 ± 15.62	92.31 ± 21.53	**<.001**
Chordae tendineae forces			
Primary, N	0.51 ± 0.17	0.10 ± 0.05	**<.001**
Secondary, N	0.41 ± 0.21	0.35 ± 0.12	.3742
Rate of change of force – primary, N/s	30.80 ± 11.38	8.59 ± 4.83	**<.001**
Rate of change of force – secondary, N/s	33.52 ± 10.59	19.07 ± 7.00	**.0060**

Data presented as mean ± standard deviation. Values in bold designate statistical significance. *RMS*, Root mean square.

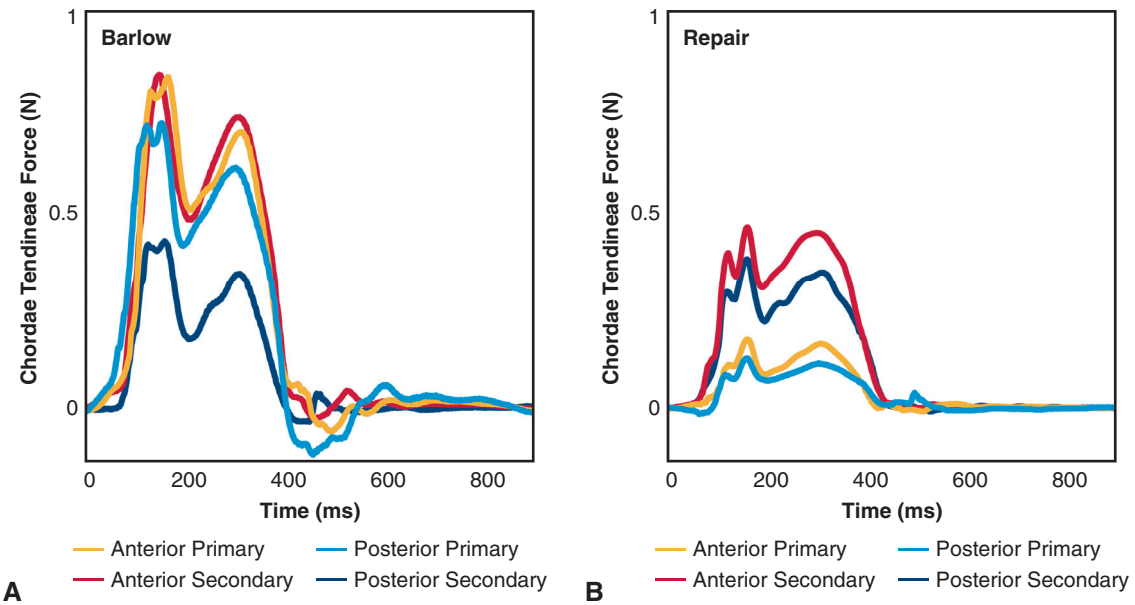

FIGURE 3. Force tracings over the course of 1 cardiac cycle for composites of each class of chordae at baseline with the Barlow's model (A) and after neochordal repair (B). Forces were measured using fiber Bragg grating strain sensors sewn to native chordae. Primary chordae forces were lower postrepair (0.51 ± 0.17 N vs 0.10 ± 0.05 N, $P < .001$), whereas no significant difference was found for secondary chordae forces (0.41 ± 0.21 N vs 0.35 ± 0.12 N, $P = .374$).

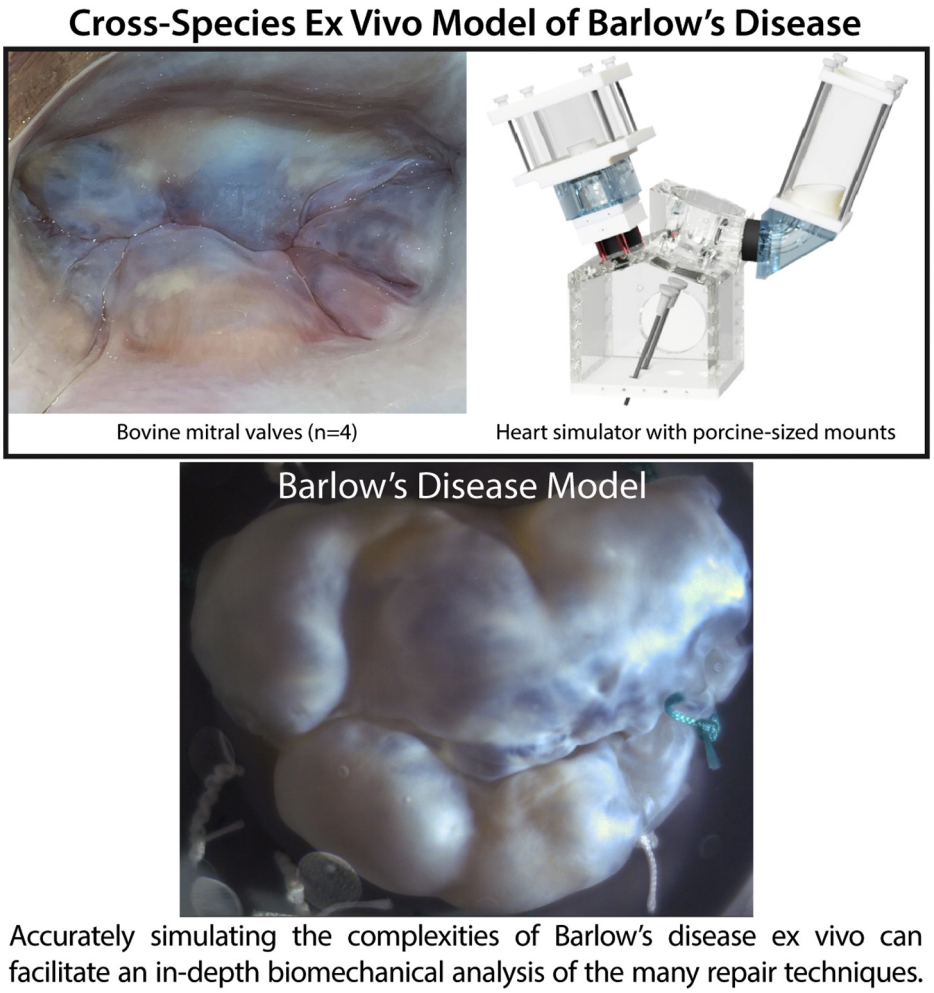

FIGURE 4. The development and biomechanical analysis of a novel cross-species model of Barlow's mitral valve disease. Bovine mitral valves (n = 4) were evaluated in a left heart simulator using porcine mounts, resulting in an ex vivo simulation of the excess, prolapsing leaflet tissue characteristic of Barlow's disease. All models were successfully repaired and tested prior to ring annuloplasty for consistency, supporting the use of this model not only as a means of analyzing the biomechanics of the disease state, but also as a tool to optimize surgical repair techniques.

DISCUSSION

A cross-species ex vivo model was successfully developed to reproduce the complexities of Barlow's disease, including redundant, billowing bileaflet tissues with notable regurgitation. After neochordal repair, hemodynamic data confirmed the restoration to physiologic conditions with significant reduction in mitral regurgitation. Strain gauge analysis revealed a sharply fluctuating force profile experienced by the elongated chordae prerepair as well as significantly lower primary chordae forces postrepair. Figure 4 depicts a summary of this study and its implications. To ensure consistency and limit any confounding factors, we elected to omit ring annuloplasty in these experiments, simulating preannuloplasty repair. Determining the effects of ring annuloplasty as well as the ideal ring geometry for the repair of Barlow's disease is an important consideration, and experiments to answer these questions are currently underway.

It has been widely theorized that in a healthy MV, primary chordae tendineae aid in positioning the leaflets to ensure proper coaptation whereas the secondary chordae support the majority of forces during systole; when a valve becomes regurgitant, the optimal coaptation surface is disrupted and the primary chordae are forced to take on additional forces.[28] This theory is reinforced by previous findings of low primary chordae forces compared with secondary chordae forces in a healthy state and postrepair.[27,29,30] In this study, we observed that the primary chordae hold forces on par with secondary chordae for a regurgitant Barlow's MV. Given that proper coaptation is not achieved during this disease state, it is likely that the primary chordae were required to hold the leaflet free edges

during systole, thus raising the primary chordae forces. Once proper coaptation was restored and the regurgitation was significantly reduced postrepair, the primary forces were lowered to their expected values.

In addition, the rate of change of force on the chordae was found to be significantly lower postrepair relative to the baseline Barlow's disease model. Note that this was the case even for secondary chordae, which had no significant difference in peak force. This difference could be due to the complex mechanics of elongated chordae coupled with a prolapsing valve. We hypothesize that the elongated chordae experience a whipping phenomenon, similar to that observed with long artificial chordae[31,32]; this phenomenon was theorized to cause a similar increased rate of change of force in longer neochords.[17] Once the Barlow's disease model is repaired, the neochords position the leaflets to ensure proper coaptation, which then cushions the initial peak in force at the start of systole by distributing the forces across the leaflets and secondary chordae. We also hypothesize that dF/dt for the neochords postrepair is likely less than the dF/dt observed for the native chordae prerepair due to the fact that the neochords are generally shorter than their adjacent chordae. The rate of change of force on the native chordae and neochords is a crucial metric in analyzing the stresses on the valve and ultimately determining the durability of a repair. Thus, great importance lies in developing an accurate disease model such that the variety of repairs can be compared, and stresses can be optimized for the repaired valve.

Limitations

One area of refinement for this model is more accurately replicating the specific papillary muscle positioning. Although consistency across levels of regurgitation was prioritized for this study, if one wishes to test a specific Barlow's disease case, the vertical displacement of the bovine papillary muscles must be selected to result in the correct length of excess chordae (ie, the difference between actual chordal length and a healthy chordal length). In addition, left ventricular dysfunction often accompanies Barlow's disease,[2] which would result in papillary muscle placement that differs from a healthy heart and may require more intricate positioning measures for accuracy. This papillary muscle simulation could be further refined through the inclusion of the ventricular interaction with the subvalvular apparatus.

The morphology and intrinsic tissue properties of the leaflet tissue are also important to consider; although our model successfully replicates the significant excess of leaflet tissue in terms of total leaflet area, it does not fully replicate the myxomatous characteristics or the thickness of human Barlow's MV. In addition, some cases of Barlow's disease can have calcification of the annular or subannular apparatus.[2] Further studies are needed to establish a mechanical or chemical treatment to the leaflets that would result in leaflet thickening, annular calcification, or other changes to the material properties of the valve. These modifications to the bovine valve could be subjected to biomechanical testing to compare the material properties with those of human Barlow's disease. Thus, although the current model can be used to study repair techniques, the ability to include more refined physiologic facets of the disease would enhance our ability to study the biomechanics of the disease itself.

CONCLUSIONS

Our novel Barlow's disease model will ultimately enable a comprehensive biomechanical analysis of the pathophysiology of the disease as well as the many repair techniques currently in use. Ex vivo simulation of valvular diseases represents an important and underused method to optimize surgical repair techniques. However, the value of these analyses is contingent on the accuracy of the disease model; this study represents an important step in developing a reliable model of Barlow's disease and enabling more accurate analyses of the surgical repair of severe MV disease.

Conflict of Interest Statement

Authors have nothing to disclose with regard to commercial support.

References

1. Barlow JB, Bosman CK. Aneurysmal protrusion of the posterior leaflet of the mitral valve. *Am Heart J*. 1966;71:166-78.
2. Anyanwu AC, Adams DH. Etiologic classification of degenerative mitral valve disease: Barlow's disease and fibroelastic deficiency. *Semin Thorac Cardiovasc Surg*. 2007;19:90-6.
3. Lawrie GM. Barlow disease: simple and complex. *J Thorac Cardiovasc Surg*. 2015;150:1078-81.
4. Lancellotti P, Moura L, Pierard LA, Agricola E, Popescu BA, Tribouilloy C, et al. European Association of Echocardiography recommendations for the assessment of valvular regurgitation. Part 2: mitral and tricuspid regurgitation (native valve disease). *Eur J Echocardiogr*. 2010;11:307-32.
5. Lawrie GM, Earle EA, Earle NR. Nonresectional repair of the barlow mitral valve: importance of dynamic annular evaluation. *Ann Thorac Surg*. 2009;88:1191-6.
6. Varghese R, Adams DH. Techniques for repairing posterior leaflet prolapse of the mitral valve. *Op Tech Thorac Cardiovasc Surg*. 2011;16:293-308.
7. da Rocha E Silva JG, Spampinato R, Misfeld M, Seeburger J, Pfanmüller B, Eifert S, et al. Barlow's mitral valve disease: a comparison of neochordal (loop) and edge-to-edge (Alfieri) minimally invasive repair techniques. *Ann Thorac Surg*. 2015;100:2127-33; discussion 2133.
8. Yano M, Nishimura M, Yokota A, Mori K. Mitral valve repair in Barlow's disease by chordal reconstruction using the adjustable slip-knot technique. *Gen Thorac Cardiovasc Surg*. 2020;68:63-6.
9. MacArthur JW, Cohen JE, Goldstone AB, Fairman AS, Edwards BB, Hornick MA, et al. Nonresectional single-suture leaflet remodeling for degenerative mitral regurgitation facilitates minimally invasive mitral valve repair. *Ann Thorac Surg*. 2013;96:1603-6.
10. Woo YJ, MacArthur JW. Posterior ventricular anchoring neochordal repair of degenerative mitral regurgitation efficiently remodels and repositions posterior leaflet prolapse. *Eur J Cardiothorac Surg*. 2013;44:485-9; discussion 489.
11. Siefert AW, Rabbah J-PM, Pierce EL, Kunzelman KS, Yoganathan AP. Quantitative evaluation of annuloplasty on mitral valve chordae tendineae forces to supplement surgical planning model development. *Cardiovasc Eng Technol*. 2014;5:35-43.

12. Fontaine AA, He S, Stadter R, Ellis JT, Levine RA, Yoganathan AP. In vitro assessment of prosthetic valve function in mitral valve replacement with chordal preservation techniques. *J Heart Valve Dis*. 1996;5:186-98.
13. Erek E, Padala M, Pekkan K, Jimenez J, Yalçinba YK, Salihoğlu E, et al. Mitral web—a new concept for mitral valve repair: improved engineering design and in-vitro studies. *J Heart Valve Dis*. 2009;18:300-6.
14. Padala M, Powell SN, Croft LR, Thourani VH, Yoganathan AP, Adams DH. Mitral valve hemodynamics after repair of acute posterior leaflet prolapse: quadrangular resection versus triangular resection versus neochordoplasty. *J Thorac Cardiovasc Surg*. 2009;138:309-15.
15. Siefert AW, Siskey RL. Bench models for assessing the mechanics of mitral valve repair and percutaneous surgery. *Cardiovasc Eng Technol*. 2015;6:193-207.
16. Paulsen MJ, Kasinpila P, Imbrie-Moore AM, Wang H, Hironaka CE, Koyano TK, et al. Modeling conduit choice for valve-sparing aortic root replacement on biomechanics with a 3-dimensional-printed heart simulator. *J Thorac Cardiovasc Surg*. 2019;158:392-403.
17. Imbrie-Moore AM, Paulsen MJ, Thakore AD, Wang H, Hironaka CE, Lucian HJ, et al. Ex vivo biomechanical study of apical versus papillary neochord anchoring for mitral regurgitation. *Ann Thorac Surg*. 2019;108:90-7.
18. Rabbah J-P, Saikrishnan N, Yoganathan AP. A novel left heart simulator for the multi-modality characterization of native mitral valve geometry and fluid mechanics. *Ann Biomed Eng*. 2013;41:305-15.
19. Vismara R, Pavesi A, Votta E, Taramasso M, Maisano F, Fiore GB. A pulsatile simulator for the in vitro analysis of the mitral valve with tri-axial papillary muscle displacement. *Int J Artif Organs*. 2011;34:383-91.
20. Al-Atassi T, Toeg HD, Jafar R, Sohmer B, Labrosse M, Boodhwani M. Impact of aortic annular geometry on aortic valve insufficiency: insights from a preclinical, ex vivo, porcine model. *J Thorac Cardiovasc Surg*. 2015;150:656-64.e1.
21. He Z, Sacks MS, Baijens L, Wanant S, Shah P, Yoganathan AP. Effects of papillary muscle position on in-vitro dynamic strain on the porcine mitral valve. *J Heart Valve Dis*. 2003;12:488-94.
22. Adams J, O'Rourke MJ. In vitro measurement of the coaptation force distribution in normal and functional regurgitant porcine mitral valves. *J Biomech Eng*. 2015;137:071008.
23. Pham T, Sun W. Material properties of aged human mitral valve leaflets. *J Biomed Mater Res A*. 2014;102:2692-703.
24. Barber JE, Kasper FK, Ratliff NB, Cosgrove DM, Griffin BP, Vesely I. Mechanical properties of myxomatous mitral valves. *J Thorac Cardiovasc Surg*. 2001;122:955-62.
25. Kavitha S. *Histomorphometric and morphological study of papillary muscles in adult human hearts. PhD Thesis*. Vinayaka Missions University; 2015.
26. Paulsen MJ, Imbrie-Moore AM, Wang H, Bae JH, Hironaka CE, Farry JM, et al. Mitral chordae tendineae force profile characterization using a posterior ventricular anchoring neochordal repair model for mitral regurgitation in a three-dimensional-printed ex vivo left heart simulator. *Eur J Cardiothorac Surg*. 2020;57:535-44.
27. Paulsen MJ, Bae JH, Imbrie-Moore A, Wang H, Hironaka C, Farry JM, et al. Development and ex vivo validation of novel force-sensing neochordae for measuring chordae tendineae tension in the mitral valve apparatus using optical fibers with embedded Bragg gratings. *J Biomech Eng*. 2020;142:014501.
28. Nazari S, Carli F, Salvi S, Banfi C, Aluffi A, Mourad Z, et al. Patterns of systolic stress distribution on mitral valve anterior leaflet chordal apparatus. A structural mechanical theoretical analysis. *J Cardiovasc Surg (Torino)*. 2000;41:193-202.
29. He Z, Jowers C. A novel method to measure mitral valve chordal tension. *J Biomech Eng*. 2009;131:014501.
30. Nielsen SL, Soerensen DD, Libergren P, Yoganathan AP, Nygaard H. Miniature C-shaped transducers for chordae tendineae force measurements. *Ann Biomed Eng*. 2004;32:1050-7.
31. Gammie JS, Wilson P, Bartus K, Gackowski A, Hung J, D'Ambra MN, et al. Transapical beating-heart mitral valve repair with an expanded polytetrafluoroethylene cordal implantation device: initial clinical experience. *Circulation*. 2016;134:189-97.
32. Lancellotti P, Radermecker M, Durieux R, Modine T, Oury C, Fattouch K. Transapical beating-heart chordae implantation in mitral regurgitation: a new horizon for repairing mitral valve prolapse. *J Thorac Dis*. 2016;8:E1665-71.

Key Words: Barlow's disease, biomechanics, mitral regurgitation, disease model, valve repair